AFRL-SR-BL-TR-98- 8

REPORT DOCUMENTATION PAGE

0673

1. AGENCY USE ONLY (Leave blank)	2. REPORT DATE	3. REPORT TYPE AND DATES COVERED
	23.09.98	Final, 15.06.98-15.09.98

4. TITLE AND SUBTITLE
Penetrator Resistance and Target Damage Due to Multiple Impacts upon Granite and Concrete: Joint Experimental, Analytical and Numerical Effort

5. FUNDING NUMBERS
US Air Force Office of Scientific Research
Contract F49620-98-C-0031

6. AUTHOR(S)
Jack Dvorkin

7. PERFORMING ORGANIZATION NAME(S) AND ADDRESS(ES)
Petrophysical Consulting, Inc.
730 Glenmere Way
Redwood City, CA 94062

8. PERFORMING ORGANIZATION REPORT NUMBER

9. SPONSORING / MONITORING AGENCY NAME(S) AND ADDRESS(ES)
Dr. Jim Cheng
AFOSR
110 Duncan Avenue, Room B115
Bolling AFB, DC 20332-8050

10. SPONSORING / MONITORING AGENCY REPORT NUMBER

11. SUPPLEMENTARY NOTES

12a. DISTRIBUTION / AVAILABILITY STATEMENT
Unlimited

DISTRIBUTION STATEMENT A
Approved for public release;
Distribution Unlimited

12b. DISTRIBUTION CODE

13. ABSTRACT (Maximum 200 words)

The overall objective of the proposed research was to fundamentally and quantitatively understand, based on first physical principles, the micromechanics of penetration into and damage accumulation in cemented particulate targets subject to multiple impact. The approach was to integrate experiments, analytical micromechanics, and numerical modeling into a concerted effort. The project was to be conducted jointly with the University of Rhode Island. The Petrophysical Consulting part of the project was analytical micromechanics. To achieve this objective we provided an elastic description of completely cemented or partially cemented granular material where the elastic properties of the grains and cement differ from each other. This new solution gives a basis for investigating the plastic deformation and failure of cemented composite targets such as concrete and granite. We also analyzed natural rock materials using acoustic pulses and deriving the strength of such materials from their elastic moduli. These results are relevant to describing the strength and damage resistance of such target geomaterials as concrete and granite. The main relevance to the Air Force mission is through a quantitative description of elastic, non-elastic, and damage accumulation properties of cemented geomaterials subject to penetrator impact.

14. SUBJECT TERMS	15. NUMBER OF PAGES
Penetration, target damage, micromechanics, particulate materials	38
	16. PRICE CODE

17. SECURITY CLASSIFICATION OF REPORT	18. SECURITY CLASSIFICATION OF THIS PAGE	19. SECURITY CLASSIFICATION OF ABSTRACT	20. LIMITATION OF ABSTRACT
Unclassified	Unclassified	Unclassified	UL

Penetrator Resistance and Target Damage Due to Multiple Impacts upon Granite and Concrete: Joint Experimental, Analytical and Numerical Effort

US AIR FORCE OFFICE OF SCIENTIFIC RESEARCH
CONTRACT F49620-98-C-0031

FINAL REPORT

PI DR. JACK DVORKIN

Petrophysical Consulting, Inc.
730 Glenmere Way
Redwood City, CA 94062
Tel. (650) 725-9296
Fax. (650) 723-1188
E-mail jack@pangea.stanford.edu

September 1998

1. SUMMARY

1.1. OBJECTIVE AND ACCOMPLISHMENTS

The overall objective of the proposed research was to (a) fundamentally and quantitatively understand, based on first physical principles, the micromechanics of penetration into and damage accumulation in cemented particulate targets subject to multiple impact; and (b) translate this understanding into a predictive code by using contact and damage laws thus derived in a DEM routine. The technical approach was to integrate experiments, analytical micromechanics, and numerical modeling into a concerted effort. The project was to be conducted jointly with the University of Rhode Island. The Petrophysical Consulting part of the project was analytical micromechanics.

To achieve this objective we continued our previous effort (AFOSR Contract F49620-96-1-0394) and provided an elastic description of completely cemented (no void) or partially cemented granular material where the elastic properties of the grains and cement differ from each other. This new result provides a solution to the problem of elastic composite with contacting inclusions -- the problem that has not been solved before. This solution gives a basis for investigating the plastic deformation and failure of cemented composite targets such as concrete and granite.

Our second achievement was in analyzing natural rock materials using acoustic pulses and deriving the strength of such materials from their elastic moduli. These results are relevant to describing the strength and damage resistance of such target geomaterials as concrete and granite.

The main relevance to the Air Force mission is through a quantitative description of elastic, non-elastic, and damage accumulation properties of cemented geomaterials subject to penetrator impact.

1.2. PERSONNEL SUPPORTED

Senior Personnel: Dvorkin, Jack, PI (US); Gary Mavko (US); and Amos Nur (US).

1.3. PUBLICATIONS

1. Jack Dvorkin, Jim Berryman, Amos Nur, and Mickaele Le Ravalec, 1998, Effective moduli of particulates with elastic cement, Mechanics of Materials, in press.
2. Jack Dvorkin, and Ivar Brevik, 1998, Diagnosing high-porosity sandstones: Strength and permeability from porosity and velocity, Geophysics, in press.
3. Per Avseth, Jack Dvorkin, Gary Mavko, and Johannes Rykkje, 1998, Diagnosing high-porosity sands for reservoir characterization using sonic and seismic, 1998 SEG Annual Conference, New Orleans, RP 2.5, 1024-1027.

1.4. INTERACTIONS AND TRANSITIONS

- 1998 Stanford Rock Physics Meeting; Stanford, CA, 1998: Natural cemented rocks.
- 1998 SEG Annual Conference, New Orleans: Diagnosing high-porosity sands for reservoir characterization using sonic and seismic.
- ASCE 1998 Meeting, La Jolla: Effective Moduli of Particulates with Elastic Cement.

1.5. PATENTS AND INVENTIONS

No patents or inventions resulted form this effort (see DD 882 attached).

2. TECHNICAL PART

In this part the technical results are presented in the form of journal articles. The numeration of formulas and figures is internal for every section.

2.1. EFFECTIVE MODULI OF PARTICULATES WITH ELASTIC CEMENT

In collaboration with Jim Berryman, Amos Nur, and Mickaele Le Ravalec

ABSTRACT

We give an approximate method for calculating the effective elastic moduli of a close random pack of identical elastic spheres whose pore space is partially or completely filled with elastic cement. To construct the solution we start with the uncemented pack and add small amounts of cement uniformly at every grain contact. The effective moduli of such an aggregate depend on those of the grains and cement (which are, generally, different), and on the amount of cement. Moduli for grain/cement mixtures are available from the contact cementation theory. Next we introduce an isotropic elastic body with void inclusions (e.g., spherical) whose porosity is the same as the porosity of the pack with contact cement. The moduli of the matrix are as yet unknown. We find them by assuming that the effective moduli of the elastic body with inclusions are equal to those of the pack with contact cement. Then an appropriate effective medium theory (e.g., self-consistent or differential effective medium approximation) provides two equations for the bulk and shear moduli of the matrix. Finally, we use the chosen effective medium theory to calculate the moduli of the elastic body with the matrix thus defined whose inclusions are now filled with the cement. We assume that these are also the moduli of the pack whose pore space is completely filled with the cement. To calculate the elastic moduli of the pack whose pore space is partially filled with the cement, we assume that they are those of the elastic body with the matrix thus defined and with two types of inclusions -- void and filled with cement (the porosity of this body

and of the cemented pack are the same). This result gives one solution to a general and previously unresolved problem of contacting elastic inclusions embedded in an elastic matrix. It provides a transition from high-porosity cemented to completely cement-filled granular materials. The solution accurately predicts the compressional elastic modulus (the product of the bulk density and P-wave velocity squared) from wave-propagation experiments on epoxy-cemented glass beads, ice-cemented Ottawa sand, and in-situ acoustic data in natural sands cemented by gas hydrate.

INTRODUCTION AND PROBLEM FORMULATION

When estimating the effective stiffness of many composites, concrete and natural rock among them, one often faces the problem of calculating the moduli of an elastic matrix with elastic inclusions. This problem has been extensively addressed in the past. The existing solutions are analyzed and summarized by, e.g., Christensen (1991), Zimmerman (1991), Wang and Nur (1992), Nemat-Nasser and Hori (1993), and Berryman (1995).

Accurate solutions are available for small inclusion concentrations and various inclusion shapes. To obtain an estimate for high concentrations, one may find the self-consistent (SC) or differential effective medium (DEM) approximations to be useful and reasonably accurate. Some fundamental solutions for composites with concentrated interacting inclusions belong to Frankel and Acrivos (1967), Goddard (1977), and Chen and Acrivos (1978).

Ju and Chen (1994) show how to calculate the effective elastic moduli of two-phase composites containing randomly dispersed spherical inhomogeneities. However, their solution does not treat the important case of spheres in direct contact and, therefore, fails to predict experimentally measured elastic moduli in such composite (see section Examples and Appendix 2).

An alternative to direct estimates is the bounding of the overall moduli of a composite (Hashin and Shtrikman, 1963). Nemat-Nasser et al. (1993) used generalized Hashin-Shtrikman variational principles to provide accurate bounds for composites with periodic microstructure. They also introduced a "modified equivalent inclusion method" for directly estimating the moduli of such composites. The results fall between the upper and lower bounds and are supported by experimental data on the shear modulus of an incompressible matrix reinforced by rigid spherical particles.

In composites with concentrated elastic inclusions, direct interaction between the inclusions through the thin layers of the matrix is very important (Goddard, 1977). The contact cementation theory (CCT) of Dvorkin et al. (e.g., 1994) highlights this conclusion. It allows one to calculate the effective elastic properties of a particulate aggregate where cement is located around the grain contacts (Figure 1a).

CCT predicts that even small volumes of contact cement (which may be soft as compared to the grains) act to strengthen the aggregate's elastic moduli, thus turning the nonlinear problem of contact analysis into a simpler linear one such as that found typically in composites analysis. The initial filling of the contact gaps is most important -- the effect of any additional cement placed around this initial filling is relatively small. This result is supported by experiments (Figure 2). Experiments also show that even by filling the entire pore space of a sphere pack one cannot achieve the drastic relative stiffness increase for which the small volumes of the contact cement are responsible.

The assumptions used in CCT make its use appropriate only for high-porosity particulates where cement is located in the immediate vicinity of the contacts. As is, CCT cannot be used to estimate the elastic constants of a zero- or low-porosity aggregate where cement fills the whole pore space (Figure 1b) or large portions of it.

Therefore, a question naturally arises: How do we calculate the effective elastic moduli of particulates where cementation extends far beyond immediate grain-to-grain contacts? Consider, for example, a close random pack of identical glass beads where the pore space is completely filled with epoxy. This aggregate is a case of contacting spherical inclusions (glass) embedded in the epoxy matrix. From CCT we know that the filling (epoxy) located at the contacts contributes most to the stiffness of the material. Then it is clear that a direct use of an inclusion theory (such as SC or DEM) is inappropriate here because it does not account for the special properties of cemented contacts. Contact cement and pore-filling cement (Figure 1c) contribute differently to the stiffness of the material.

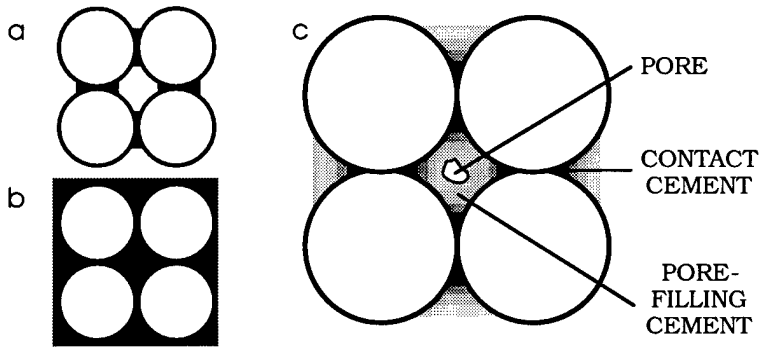

Figure 1. a. Grains with contact cement. b. Grains with pore space completely filled. c. Contact cement and pore-filling cement.

To treat this problem our approach is to obtain a solution to the concentrated inclusion problem (the bulk and shear moduli of a close random pack of identical elastic spheres whose pore space is partially or completely filled with elastic cement) where the (previously ignored) special properties of the contact-cement part of the matrix are recognized and included. The problem posed is important, not only methodologically, because many cemented geomaterials, such as, e.g., concrete, have inclusion concentrations close to the upper limit, small void concentration (porosity) and large amounts of pore-filling cement.

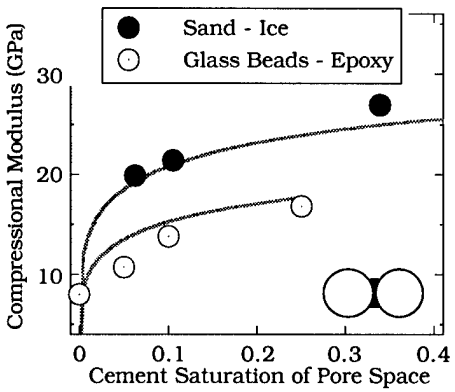

Figure 2. CCT theoretical predictions (curves) and experimental data (symbols) for the compressional elastic modulus from elastic wave propagation experiments. The cemented samples were prepared by (a) adding epoxy to a close random pack of identical glass beads (Yin, 1993), and (b) adding water to Ottawa sand and then freezing it (Tutuncu, 1997). Both epoxy and water are wetting fluids and, when they solidify, act as contact cement in the form of pendular rings. The modulus is plotted versus the cement saturation of the pore space of the uncemented glass bead and sand packs.

SOLUTION

To solve this problem, we assume that at some high porosity where CCT is still applicable (Figure 3, point B), the effective bulk and shear moduli of the cemented material are those of a homogeneous isotropic matrix with empty spherical inclusions of the same porosity. Next we use an effective medium theory, for example, SC (Berryman, 1980) or DEM (Norris, 1985), to express these effective bulk and shear moduli through the, as yet unknown, elastic moduli of the hypothetical matrix material. Then the elastic moduli of the matrix material can be found from the two resulting equations.

To find the elastic moduli of the sphere pack where the entire pore space is filled with cement, we assume that they are the same as those of the hypothetical matrix whose inclusions are now completely filled with the cement (Figure 3, point C). Those moduli can be computed using the chosen effective medium theory.

Finally, we find the moduli of the cemented sphere pack of a non-zero porosity by assuming that they are those of the cement-filled hypothetical matrix into which empty

spherical inclusions are embedded (Figure 3, point D). The porosities of this new body with inclusions and of the cemented pack are the same.

The mathematical expressions for this algorithm are given in Appendix 1.

Of course, the inclusions do not have to be spherical (results for ellipsoidal-shaped inclusions are easily obtained within the same approach), and effective medium theories other than SC and DEM could be used.

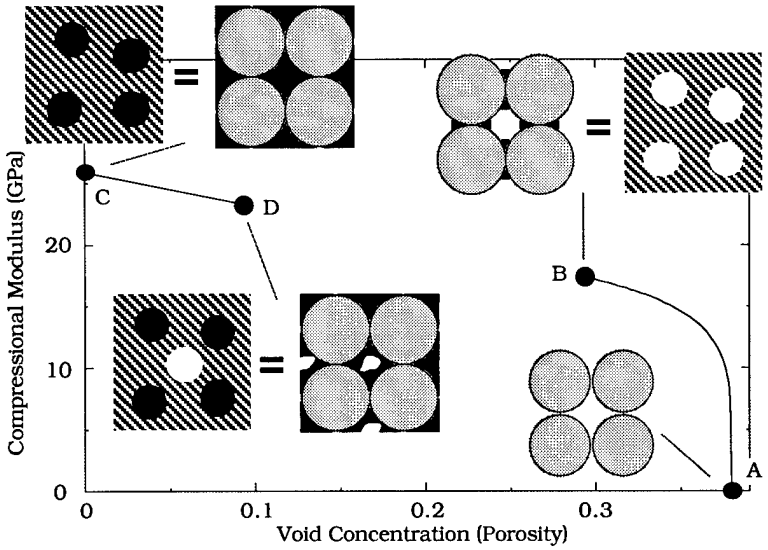

Figure 3. Proposed solution scheme. "A", uncemented sphere pack of zero stiffness. "B", pack with small volume of contact cement whose moduli are calculated from CCT; the moduli of the hypothetical matrix material are found from SC or DEM. "C", completely cemented matrix and sphere pack. "D", matrix and sphere pack of non-zero porosity. The graph (compressional modulus versus porosity) is given for epoxy-cemented glass beads.

EXAMPLES

In the examples below, the compressional modulus M is calculated from the measured P-wave velocity V_p and bulk density ρ as $M = \rho V_p^2$. In the laboratory experiments presented here, the shear-wave velocity has been recorded as well. We do not use these experimental results because the quality of the shear-wave data was (traditionally) poor due to the interference of converted P-waves. The wave-length in all

the experiments is much larger that the individual grain size, which justifies the effective medium approach to the problem.

The elastic properties of materials (glass, quartz, epoxy, and ice) used in the calculations are given in Table 1.

Table 1. Elastic moduli of materials used in calculations.

Material	Shear Modulus (GPa)	Bulk Modulus (GPa)
Glass	30.34	45.55
Epoxy	2	6.8
Quartz	45	36.6
Ice	3.53	8.57
Gas Hydrate	2.4	5.6

LABORATORY EXPERIMENTS. The elastic-wave velocities have been measured in glass bead packs cemented with epoxy by Yin (1993), and in water-saturated and frozen pure-quartz Ottawa sand by Tutuncu (1997). Both liquid epoxy and water are wetting fluids and tend to accumulate at grain contacts. Therefore, at high porosity CCT is applicable to estimating the effective elastic moduli of the aggregates under examination.

At low porosity we use the above-described solution with SC (Berryman, 1980) and DEM (Norris, 1985) approximations for spherical inclusions. In both cases our theoretical estimates match the experimental data well (Figure 4).

An adjustable parameter in the solution is porosity above which CCT is used and below which the new solution is employed. Our solution is stable with respect to this parameter (see Figure 5 for epoxy-cemented glass beads) and, therefore, this transition porosity can be arbitrarily chosen within the reasonable limits where CCT is applicable.

It would be more satisfying if all of the new solution curves intersected the zero porosity axis at the same modulus value, but instead we find that the present formulation of the theory produces a set of curves that are shifted (more or less) in parallel depending on their point of intersection with the CCT curve. This result

suggests that the current formulation might be improved using a more sophisticated effective medium method.

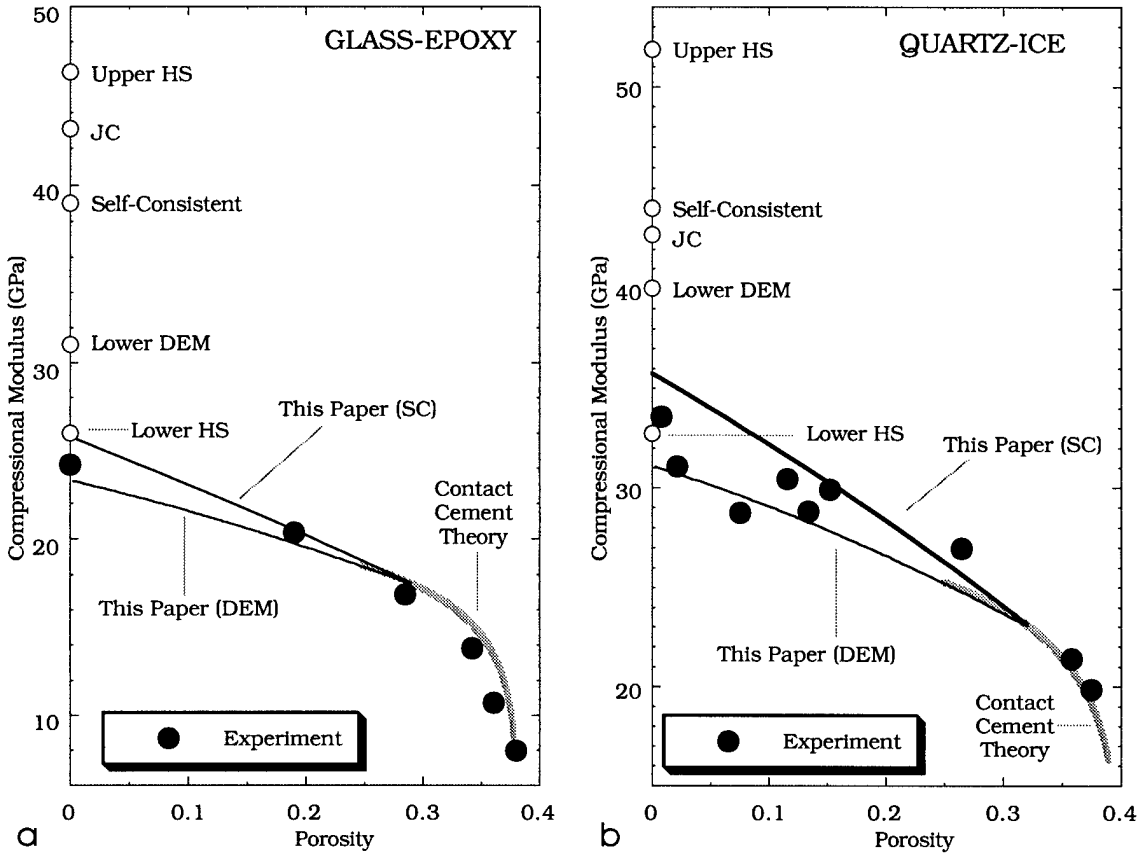

Figure 4. Compressional modulus versus porosity for (a) epoxy-cemented glass beads, and (b) ice-cemented Ottawa sand. Filled symbols are from the experiments. Curves are from theory. Open symbols show the results of applying effective-medium theories to the grain-cement mixture at zero void concentration.

The most important result of our new solution is the elastic moduli of cemented spheres at zero void concentration. In order to show that it is crucial to account for the specific geometry (contacting spheres) of the aggregate, we compare this solution to various two-component effective medium results. We use the Hashin-Shtrikman (1963) bounds (Upper HS and Lower HS), SC (Berryman, 1980), Lower DEM (Norris, 1985), and the Ju and Chen (1994) solution (JC) to directly mix cement and spheres at zero void porosity. The results are shown in Figure 4 and given in Table 2. Only the Lower HS

values appear to well match the experimental data and our new solution. This is consistent with the geometry of the aggregates under examination where softer cement envelopes stiffer grains. All other effective medium theories fail to match the experimental data.

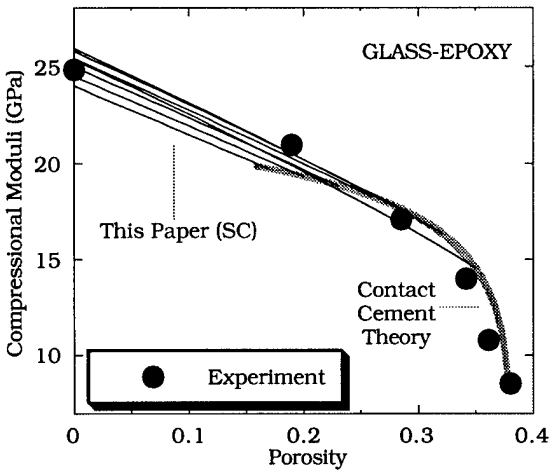

Figure 5. Stability of the new solution. Compressional modulus of epoxy-cemented glass beads versus porosity. Bold curve are from CCT, thin lines are from our new solution (SC). These lines start at a varying transitional porosity.

Table 2. Applying various effective-medium theories at zero porosity.

Compressional Modulus (GPa)	Glass-Epoxy	Quartz-Ice
Experiment	24.2	34.0
This Paper	25.4	35.7
SC	39.0	44.0
Lower DEM	31.	40.0
Upper HS	46.3	51.9
Lower HS	26.0	32.7
JC	43.1	42.7

IN-SITU MEASUREMENTS. Gas hydrate is an ice-like substance resulting from a reaction between methane and water in a favorable temperature and pressure range. Hydrates discovered in nature often fill the pore space in natural rocks and cement the rock grains. An example presented here is based on in-situ velocity, porosity, and gas-hydrate saturation measurements conducted in a well drilled through sandy intervals in the North Slope of Alaska (Mathews, 1986).

In Figure 6 we give the porosity of the rock frame (without gas hydrate), volumetric fraction of gas hydrate in the pore space (from electrical measurements), and the compressional-wave velocity as measured in situ by well logging tools.

The acoustic data is compared to our theoretical prediction (Figure 6c). In this case we used our new solution with SC approximation. The match between the data and theory is very good.

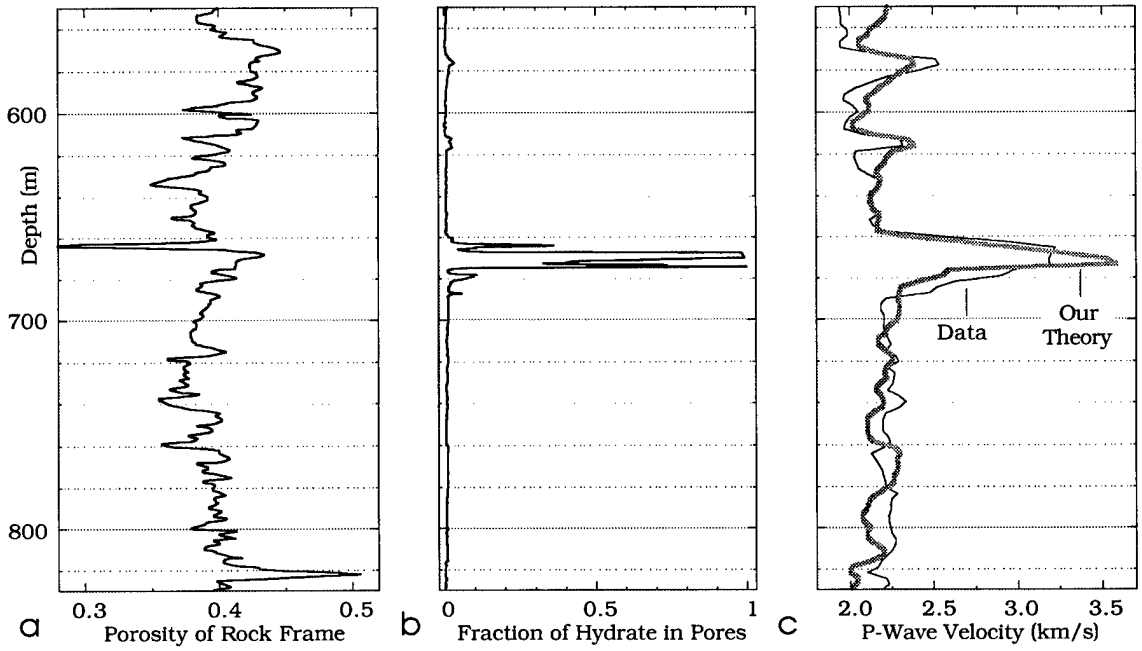

Figure 6. Porosity (a), gas hydrate concentration (b), and compressional-wave velocity (c) versus depth in a gas hydrate well.

CONCLUSION

We calculate the effective moduli of an elastic matrix with elastic inclusions at high concentration by modeling it as a cemented particulate aggregate. This approach allows us to account for the important role of the contact cement part of the matrix and address the problem of directly contacting inclusions. The latter problem cannot be approached using traditional solutions where the inclusions are considered absolutely

rigid (e.g., Frankel and Acrivos, 1967) and separated by a finite-thickness layer of the matrix.

The solution is a combination of the contact cementation theory and an effective medium theory such as the self-consistent or differential effective medium approximation. The solution is approximate because it uses a number of assumptions. Nevertheless, its predictions are confirmed by experimental data on cemented glass beads, sand, and natural rocks. We are able to accurately model the dynamic compressional moduli of these aggregates. None of the existing effective-medium solutions can adequately match the experimental results.

One legitimate criticism of the present formulation of the theory is that neither of the two effective medium theories used, although well-established and relatively easy to use, permits the user to control the microstructure of the resulting composite in any substantial way. In particular, both approaches when applied in Steps 3 and 4 (see Appendix) will surely violate our assumed microstructure for intermediate porosities by effectively placing voids in the grains (where we do not want them) as well as in the cement material (where we really do want them to be).

This effect will be comparatively small when the cementing material has similar or the same elastic parameters as the grains as is the case for our glass-glass and quartz-quartz examples. But it may have a substantial effect on the predicted properties in the cases where the ratio of grain to cement properties is large as is the case for glass-epoxy and quartz-ice. The expected bias that would result from the undesired voids in the grains is that the predicted effective values of the grain/cement mixture at zero porosity must contain a higher proportion of grain material in the total volume than that present in the CCT calculations. The result will be a bias towards higher than realistic values at zero porosity and this is exactly what we observe for the SC theory in the

glass-epoxy and quartz-ice examples. From this point of view, the present results should be considered preliminary; we need to continue searching for relatively simple effective medium theories that will permit us to gain control over the microstructure being modeled.

Still, this solution can be directly applied to estimating the stiffness of particulates such as concrete where the grains touch each other and the void fraction is small.

REFERENCES

Berge, P.A., Berryman, J.G., and Bonner, B.P., 1993, Influence of microstructure on rock elastic properties, Geophys. Res. Lett., 20, 2619-2622.

Berryman, J.G., 1980, Long-wavelength propagation in composite elastic media, I and II, J. Acoust. Soc. Amer., 68, 1809-1831.

Berryman, J.G., 1995, Mixture theories for rock properties, in Rock Physics and Phase Relations, T.J. Ahrens, ed., AGU Reference Shelf 3, AGU, Washington, DC., 205-228.

Berryman, J.G., and Berge, P.A., 1996, Critique of two explicit schemes for estimating elastic properties of multiphase composites, Mechanics of Materials, 22, 149-164.

Chen, H.-S., and Acrivos, A., 1978, The effective elastic moduli of composite materials containing spherical inclusions at non-dilute concentrations, Int. J. Solids Structures, 14, 349-361.

Christensen, R.M., 1991, Mechanics of Composite Materials, Krieger Publishing Company, Malabar, Florida.

Dvorkin, J., Nur, A. and Yin, H., 1994, Effective properties of cemented granular material, Mechanics of Materials, 18, 351-366.

Dvorkin, J., and Nur, A., 1996, Elasticity of high-porosity sandstones: Theory for two north sea datasets, Geophysics, 61, 1363-1370.

Frankel, N.A., and Acrivos, A., 1967, On the viscosity of a concentrated suspension of solid spheres, Chem. Eng. Sci., 22, 847-853.

Goddard, J.D., 1977, An elastodynamic theory for the rheology of concentrated suspensions of deformable particles, Proc. R. Soc. Lond., A 430, 105-131.

Han, D.-H., 1986, Effects of porosity and clay content on acoustic properties of sandstones and unconsolidated sediments: Ph.D. thesis, Stanford University.

Hashin, Z., and Shtrikman, S., 1963, A variational approach to the elastic behavior of multiphase materials: J. Mech. Phys. Solids, 11, 127-140.

Ju, J.W., and Chen, T.M., 1994, Effective elastic moduli of two-phase composites containing randomly dispersed spherical inhomogeneities, Acta Mechanica, 103, 123-144.

Mathews, M., 1986, Logging characteristics of methane hydrate, The Log Analyst, May-June 1986, 26-62.

Nemat-Nasser, S., and Hori, M., 1993, Micromechanics: Overall Properties of Heterogeneous materials, North-Holland, Amsterdam.

Nemat-Nasser, S., Yu, N., and Hori, M., 1993, Bounds and estimates of overall moduli of composites with periodic microstructure, Mechanics of Materials, 15, 163-181.

Norris, A.N., 1985, A differential scheme for the effective moduli of composites, Mechanics of Materials, 4, 1-16.

Strandenes, S., 1991, Rock physics analysis of the Brent Group Reservoir in the Oseberg Field: Stanford Rock Physics and Borehole Geophysics Project.

Tutuncu, A.N., 1997, Personal communication.

Wang, Z., and Nur, A. (eds.), 1992, Seismic and Acoustic Velocities in Reservoir Rocks, 2, SEG, Tulsa, Oklahoma.

Yin, H., 1993, Acoustic Velocity and Attenuation of Rocks: Isotropy, Intrinsic Anisotropy, and Stress Induced Anisotropy, Ph.D. thesis, Stanford University.

Zimmerman, R.W., 1991, Compressibility of Sandstones, Elsevier, Amsterdam.

APPENDIX 1: SOLUTION ALGORITHM

Step 1, Contact Cementation Theory (CCT). The effective compressional (M_{CCT}), bulk (K_{CCT}), and shear (G_{CCT}) moduli of a random dense pack of identical spheres cemented at their contacts are (Dvorkin and Nur, 1996):

$$K_{CCT} = \frac{n(1-\phi_0)}{6} M_c S_n, \quad G_{CCT} = \frac{3}{5} K_{CCT} + \frac{3n(1-\phi_0)}{20} G_c S_\tau, \quad M_{CCT} = K_{CCT} + \frac{4}{3} G_{CCT};$$

where M_c and G_c are the compressional and shear moduli of the cement respectively; $\phi_0 \approx 0.36$ is the porosity of the uncemented pack; and $n \approx 8.5$ is the average number of contacts per grain.

Parameters S_n and S_τ are:

$$S_n = A_n(\Lambda_n)\alpha^2 + B_n(\Lambda_n)\alpha + C_n(\Lambda_n),\ A_n(\Lambda_n) = -0.024153 \cdot \Lambda_n^{-1.3646},$$
$$B_n(\Lambda_n) = 0.20405 \cdot \Lambda_n^{-0.89008},\ C_n(\Lambda_n) = 0.00024649 \cdot \Lambda_n^{-1.9864};$$
$$S_\tau = A_\tau(\Lambda_\tau, \nu)\alpha^2 + B_\tau(\Lambda_\tau, \nu)\alpha + C_\tau(\Lambda_\tau, \nu),$$
$$A_\tau(\Lambda_\tau, \nu) = -10^{-2} \cdot (2.26\nu^2 + 2.07\nu + 2.3) \cdot \Lambda_\tau^{0.079\nu^2 + 0.1754\nu - 1.342},$$
$$B_\tau(\Lambda_\tau, \nu) = (0.0573\nu^2 + 0.0937\nu + 0.202) \cdot \Lambda_\tau^{0.0274\nu^2 + 0.0529\nu - 0.8765},$$
$$C_\tau(\Lambda_\tau, \nu) = 10^{-4} \cdot (9.654\nu^2 + 4.945\nu + 3.1) \cdot \Lambda_\tau^{0.01867\nu^2 + 0.4011\nu - 1.8186};$$
$$\Lambda_n = \frac{2G_c}{\pi G} \frac{(1-\nu)(1-\nu_c)}{1-2\nu_c},\ \Lambda_\tau = \frac{G_c}{\pi G};$$

where G and ν are the shear modulus and the Poisson's ratio of the grain material, respectively; and ν_c is the Poisson's ratio of the cement. Parameter α is

$$\alpha = 2\left[\frac{\phi_0 - \phi}{3n(1-\phi_0)}\right]^{0.25};$$

ϕ is the porosity of the cemented aggregate which is smaller than ϕ_0 because of cement deposited in the pore space of the sphere pack.

Step 2, Self-Consistent Approximation (SC). If the moduli K_s and G_s of the hypothetical matrix material were known, then the self-consistent approximation for

spherical inclusions of void with concentration ϕ predicts that K_{CCT} and G_{CCT} are given by the coupled equations (Berryman, 1980):

$$\frac{1}{K_{CCT}+\frac{4}{3}G_{CCT}} = \frac{1-\phi}{K_s+\frac{4}{3}G_{CCT}} + \frac{\phi}{\frac{4}{3}G_{CCT}},$$

$$\frac{1}{G_{CCT}+Z} = \frac{1-\phi}{G_s+Z} + \frac{\phi}{Z}, \quad Z = \frac{G_{CCT}(9K_{CCT}+8G_{CCT})}{6(K_{CCT}+2G_{CCT})}.$$

These equations have to be solved iteratively to find K_{CCT} and G_{CCT} when K_s and G_s are known. But, since K_{CCT} and G_{CCT} are already given in Step 1, we may solve the two equations instead for K_s and G_s. Solving in this direction, the equations decouple and provide explicit, unique results for K_s and G_s.

Step 2', Differential Effective Medium Approximation (DEM). In this case K_s and G_s can be found from the following two equations (Norris, 1985):

$$\frac{G_{CCT}}{G_s} = (1-\phi)^2\left[\frac{1.5+\lambda_s G_{CCT}/G_s}{1.5+\lambda_s}\right]^{\frac{1}{3}}, \quad \frac{K_{CCT}}{K_s} = \frac{G_{CCT}}{G_s}\frac{0.75+\lambda_s}{0.75+\lambda_s(G_{CCT}/G_s)^{\frac{3}{5}}};$$

where

$$\lambda_s = \frac{3(1-5\nu_s)}{4(1+\nu_s)}, \quad \nu_s = \frac{1}{2}\frac{3K_s-2G_s}{3K_s+G_s}.$$

Norris' result can be rewritten to show explicitly that

$$\lambda_s = \lambda_{CCT}(1-\phi)^{-\frac{6}{5}}\left(\frac{1.5+\lambda_s}{1.5+\lambda_{CCT}}\right)^{\frac{1}{5}},$$

where

$$\lambda_{CCT} = \frac{3(1-5\nu_{CCT})}{4(1+\nu_{CCT})}, \quad \nu_{CCT} = \frac{1}{2}\frac{3K_{CCT}-2G_{CCT}}{3K_{CCT}+G_{CCT}}.$$

Although this is an implicit equation relating λ_s to λ_{CCT} (and therefore must be solved iteratively), we can see that the equation is "almost" explicit by noting that ν_{CCT} $\approx$ 0.2 is often a good approximation for porous media. Then both λ_s and λ_{CCT} will be

small in magnitude and, therefore, the last factor in the right-hand side of the equation will be closely approximated by unity. Thus λ_s is uniquely determined by λ_{CCT} and ϕ in the expected range of the elastic parameters for porous materials.

Step 3 and 4, SC. The moduli K_{Fill} and G_{Fill} of the matrix where all inclusions (of concentration ϕ) are filled with the cement can be found from the following two equations (Berryman, 1980):

$$(1-\phi)(K_s - K_{Fill})P_s + \phi(K_c - K_{Fill})P_c = 0,$$
$$(1-\phi)(G_s - G_{Fill})Q_s + \phi(G_c - G_{Fill})Q_c = 0,$$

where

$$P_s = \frac{K_{Fill} + 4/3\, G_{Fill}}{K_s + 4/3\, G_{Fill}}, \quad P_c = \frac{K_{Fill} + 4/3\, G_{Fill}}{K_c + 4/3\, G_{Fill}},$$
$$Q_s = \frac{G_{Fill} + Z}{G_s + Z}, \quad Q_c = \frac{G_{Fill} + Z}{G_c + Z}, \quad Z = \frac{G_{Fill}(9K_{Fill} + 8G_{Fill})}{6(K_{Fill} + 2G_{Fill})}.$$

Next we calculate the effective moduli (K_{Eff} and G_{Eff}) of the same matrix where some of the inclusions are filled with the cement, and some are empty. If the concentration of the empty inclusions is ϕ_e, the concentration of the cemented inclusions is $\phi - \phi_e$ because the volumetric fraction of the matrix is still $1-\phi$. The desired moduli are found from the following two equations:

$$(1-\phi)(K_s - K_{Eff})P_s + (\phi - \phi_e)(K_c - K_{Eff})P_c - \phi_e K_{Eff} P_0 = 0,$$
$$(1-\phi)(G_s - G_{Eff})Q_s + (\phi - \phi_e)(G_c - G_{Eff})Q_c - \phi_e G_{Eff} Q_0 = 0,$$

where

$$P_s = \frac{K_{Eff} + 4/3\, G_{Eff}}{K_s + 4/3\, K_{Eff}}, \quad P_c = \frac{K_{Eff} + 4/3\, G_{Eff}}{K_c + 4/3\, G_{Eff}}, \quad P_0 = \frac{K_{Eff} + 4/3\, G_{Eff}}{4/3\, G_{Eff}},$$
$$Q_s = \frac{G_{Eff} + Z}{G_s + Z}, \quad Q_c = \frac{G_{Eff} + Z}{G_c + Z}, \quad Q_0 = \frac{G_{Eff} + Z}{Z}, \quad Z = \frac{G_{Eff}(9K_{Eff} + 8G_{Eff})}{6(K_{Eff} + 2G_{Eff})}.$$

Steps 3' and 4', DEM. We use the iterative scheme developed by Norris (1985). We choose a volumetric fraction increment $d\phi$ such that $d\phi << \phi$. The total number of iterations N is (Zimmerman, 1991):

$$N = -\frac{\ln(1-\phi)}{d\phi}.$$

The number of the first N_e steps is $N_e = N\phi_e / \phi$. During these iterations we calculate the effective bulk K_{Eff} and shear G_{Eff} moduli as:

$$K_{Eff}^{(j+1)} = K_{Eff}^{(j)} - \frac{K_{Eff}^{(j)}(4G_{Eff}^{(j)} + 3K_{Eff}^{(j)})}{4G_{Eff}^{(j)}} d\phi,$$

$$G_{Eff}^{(j+1)} = G_{Eff}^{(j)} - \frac{G_{Eff}^{(j)}(15K_{Eff}^{(j)} + 20G_{Eff}^{(j)})}{9K_{Eff}^{(j)} + 8G_{Eff}^{(j)}} d\phi;$$

$$K_{Eff}^{(0)} = K_s, \quad G_{Eff}^{(0)} = G_s.$$

The last $N - N_e$ iterations are performed using equations

$$K_{Eff}^{(j+1)} = K_{Eff}^{(j)} + \frac{(K_c - K_{Eff}^{(j)})(4G_{Eff}^{(j)} + 3K_{Eff}^{(j)})}{4G_{Eff}^{(j)} + 3K_c} d\phi,$$

$$G_{Eff}^{(j+1)} = G_{Eff}^{(j)} + \frac{(G_c - G_{Eff}^{(j)})(15K_{Eff}^{(j)} + 20G_{Eff}^{(j)})}{9K_{Eff}^{(j)} + 8G_{Eff}^{(j)} + 6(K_{Eff}^{(j)} + 2G_{Eff}^{(j)})G_c / G_{Eff}^{(j)}} d\phi.$$

APPENDIX 2: COMPARISON OF VARIOUS EFFECTIVE MEDIUM SOLUTIONS

Below, we compare the results of various effective medium theories (see text for the meaning of abbreviations) for two-phase composites made of (a) glass and epoxy, and (b) quartz and ice. The vertical lines in the graphs correspond to the volumetric fraction of 0.36 which is approximately the fraction of cement in the case where the spherical inclusions touch each other. Only the Lower HS limit comes close to the experimental results and our new solution (see Figure 4).

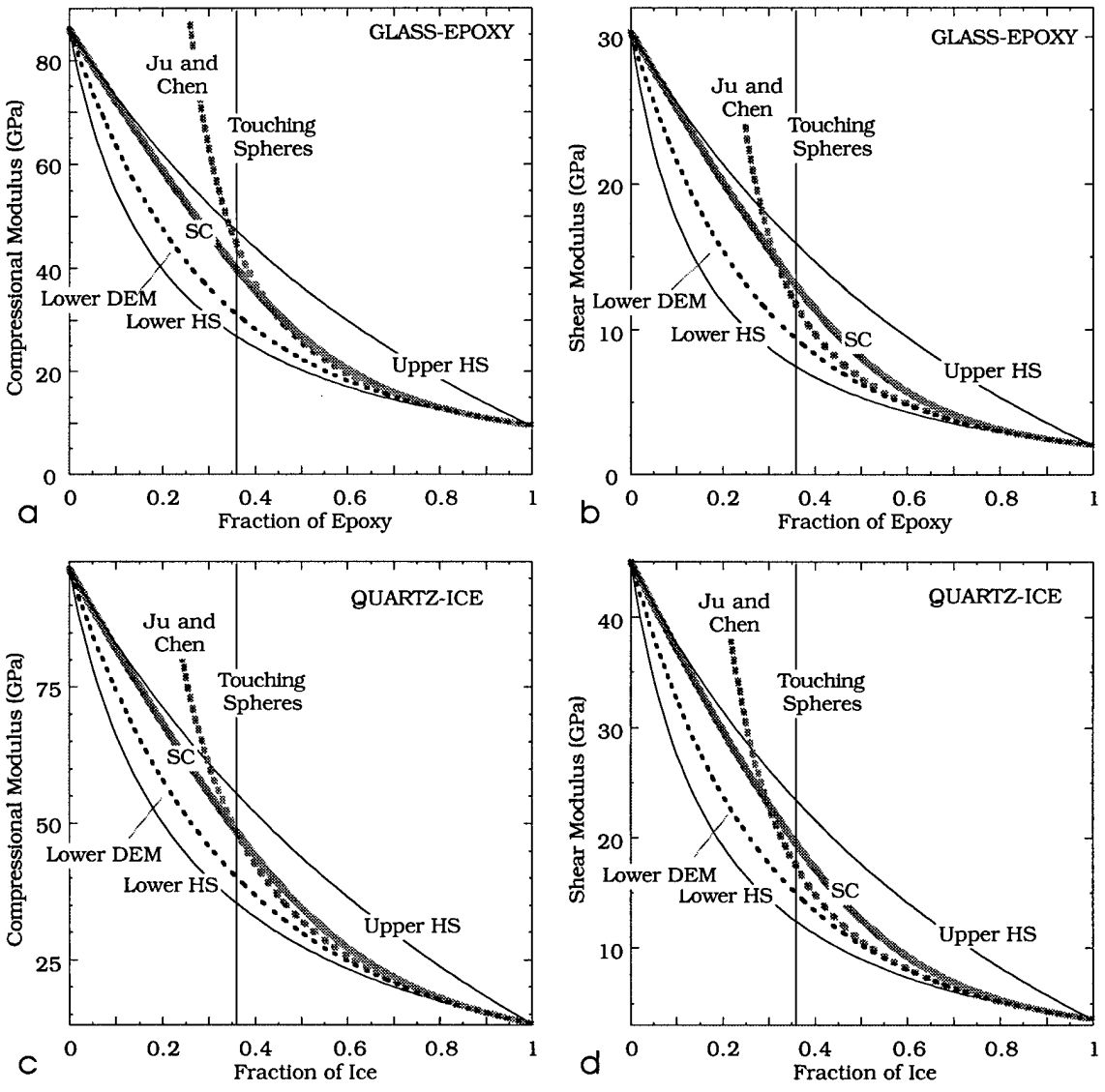

Figure 7. Compressional and shear moduli of two-phase composites as given by various effective medium theories.

2.2. DIAGNOSING SANDSTONES: STRENGTH AND PERMEABILITY FROM POROSITY AND VELOCITY

In collaboration with Ivar Brevik

INTRODUCTION

Non-uniqueness in relating velocity to porosity in core and well-log data complicates interpretation of sonic and seismic measurements. One reason for this non-uniqueness in sandstones is clay (e.g., Han, 1986). Another reason is textural variability among samples. Dvorkin and Nur (1996) examine two relatively clay-free sandstone groups in the same porosity range, but whose velocities significantly differed (Figure 1a). By comparing the data with effective-medium theories they interpret this velocity difference as resulting from the difference in the position of diagenetic cement. The explanation is that in the "fast" (Oseberg) rocks (contact) cement is located predominantly at the grain contacts whereas in the "slow" (Troll) rocks (non-contact) cement is located predominantly away from these contacts.

Coincidentally, the permeability of the Troll rocks is smaller than that of the Oseberg rocks (Figure 1b). This fact allows us to assume that the position of the diagenetic cement affects not only velocity but also permeability. The assumption is supported by numerical simulations of Bosl et al. (1998). This effect has a simple physical explanation: the non-contact cement acts to increase the specific surface area (Figure 1b) and thus decrease permeability.

Consider now a dataset where a clear trend between porosity and permeability is absent. Our working hypothesis is that this may be due to the variability in the location of diagenetic cement. We use this hypothesis in a case study where permeability and porosity data are available from cores in a well and velocity is available from a sonic log. A relationship between permeability and porosity is absent. The goal is to find a textural property of high-porosity sandstones with which permeability correlates well.

To do so, we use log-derived velocity and porosity together with rock physics theory to subdivide the diagenetic cement into the contact and non-contact parts. Then by relating permeability to the volumetric fraction of the non-contract cement in the rock we obtain a usable trend. This non-contact cement fraction is the desired textural property.

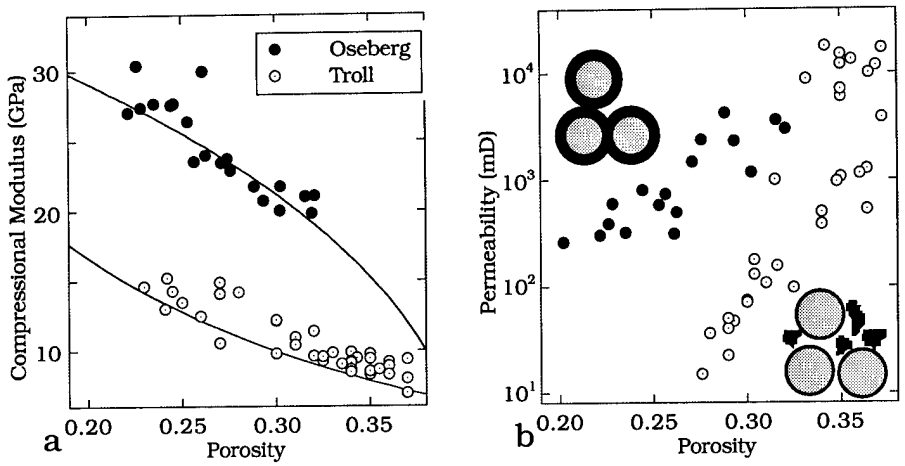

Figure 1. a. Compressional modulus (the product of bulk density and P-wave velocity squared) versus porosity for the Oseberg and Troll samples. The data displayed are for room-dry rocks at 30 MPa effective pressure (Strandenes, 1991; and Blangy, 1992). The upper curve is from the contact cement theory and the bottom curve is from the non-contact cement theory (Dvorkin and Nur, 1996). b. Permeability versus porosity for the same datasets (Strandenes, 1995). The cartoons schematically show the location of cement among grains (contact for Oseberg and non-contact for Troll).

By quantifying the amount of contact and non-contact cement we diagnose sandstone's texture from well log data, similar to Dvorkin and Nur (1998). We show that such diagnostic is important not only for obtaining a high-correlation permeability trend but also for assessing the strength of the rock.

NORTH SEA SLEIPNER FIELD, WELL 15/9-16

A vertical well, 15/9-16, penetrates the North Sea Sleipner gas/condensate reservoir comprised of Paleocene turbiditic sand. Porosity and permeability are available from

about 60 plugs that evenly cover the interval from 2380 to 2460 m. The vertical and horizontal permeabilities are practically identical. The latter is used in this study. The sandstone is very well sorted with the average sorting coefficient of 1.7; grain size varies between 0.15 and 0.25 mm. The grains are predominantly quartz (average 80%) with the rest being feldspar (average 14%), mica (average 2.3%), and clay, mostly chlorite, (average 2.2%). Traces of calcite and other minerals are also present. The contact cement in these rocks is quartz (Nadeau, 1998).

The upper part of the well is saturated with gas, with the gas-water contact at 2430 m. The bulk moduli and densities of the formation water and gas are 2.75 GPa and 1.02 g/cm^3, and 0.07 GPa and 0.27 g/cm^3, respectively (calculated using Batzle and Wang, 1992).

The interval under investigation can be subdivided into a high-resistivity zone (HRZ) overlaying a low-resistivity zone (LRZ) with the transition at about 2410 m (Figure 2a). Nadeau (1998) shows that there is a diagenetic change associated with this transition. HRZ has a restricted distribution of diagenetic chlorite and up to 5% quartz cement. LRZ has a slightly larger content of chlorite and a smaller degree of cementation.

Porosity in the entire interval is high. We calculate it from bulk density (Schlumberger, 1989). It's values do not differ much from those measured on cores except for a few points in LRZ (Figure 2b). The final results of this study practically do not depend on what porosity (log-derived or core) we use. For this reason we relate all parameters to the log-derived porosity.

The available log data contain only compressional-wave velocity. We calculate the dry-frame compressional modulus (the product of bulk density and P-wave velocity squared) by the V_p-only fluid substitution method of Mavko et al. (1995). The result is well matched by the values measured on several selected room-dry plugs (Figure 2d). The

30 MPa effective pressure for these datapoints essentially equals the reservoir effective pressure (about 29 MPa).

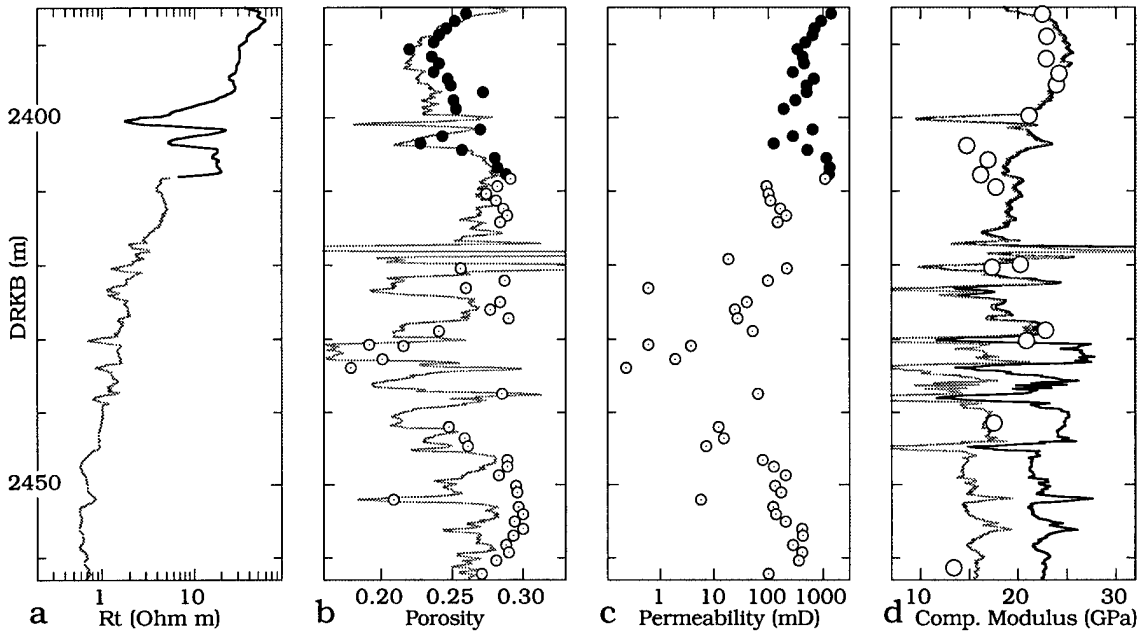

Figure 2. Various parameters versus depth in well 15/9-16. a. Far resistivity. Gray curve is for LRZ. b. Log-derived (gray curve) and core porosity. Open symbols are for LRZ. c. Permeability. Open symbols are for LRZ. d. Dry-rock (gray curve) and directly measured (black curve) compressional modulus. Symbols are from dry-rock lab measurements at 30 MPa.

ANALYSIS OF DATA

There is a very weak and practically not useful correlation between permeability and porosity (either log-derived or core) in well 15/9-16 (Figure 3). This fact can also be observed in Figures 2b and 2c where porosity and permeability are plotted versus depth. The lower-porosity sandstones in HRZ have permeability larger than that of the higher-porosity sandstones in LRZ. Notice also that the LRZ sandstones are softer than the HRZ sandstones (Figure 2d).

The modulus-porosity and permeability-porosity trends for HRZ and LRZ are given in Figure 4. In the modulus-porosity plane (Figure 4a) the HRZ trend parallels that of the contact-cemented Oseberg rocks and the contact cement theoretical trajectory (the latter

calculated for quartz grains with quartz cement). The HRZ rocks have a tight modulus-porosity trend. Remarkably, in the permeability-porosity plane (Figure 4b) the HRZ sandstones plot on top of the Oseberg data and also exhibit a noticeable permeability-porosity trend.

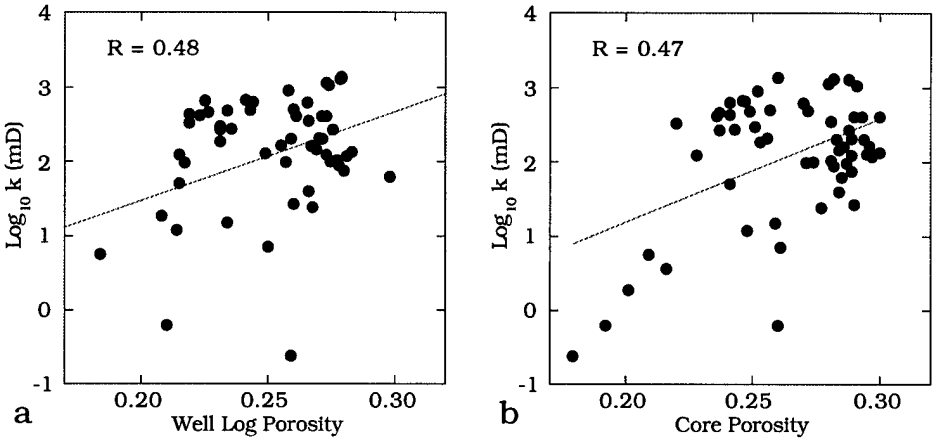

Figure 3. Horizontal permeability versus log-derived (a) and core (b) porosity. Gray lines show best linear fits. Correlation coefficients are given in the graphs.

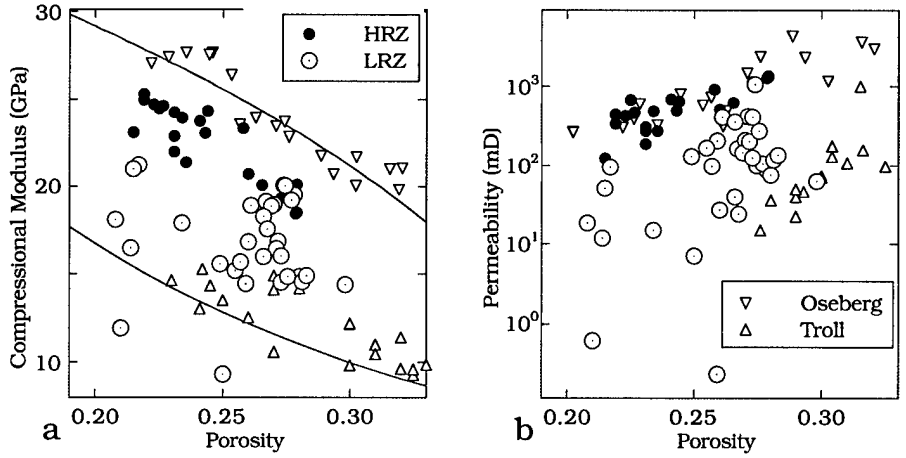

Figure 4. a. Dry-frame compressional modulus versus porosity for the Oseberg and Troll samples at 30 MPa, and HRZ and LRZ. The HRZ and LRZ data are selected at the depths of permeability datapoints. The upper curve is from the contact cement theory and the bottom curve is from the non-contact cement theory. b. Permeability versus porosity for the same datasets. The open triangles are for Oseberg and Troll. The filled circles are for HRZ and the open circles are for LRZ. The Oseberg and Troll data are plotted versus core porosity whereas the HRZ and LRZ data are plotted versus log-derived porosity.

The LRZ sandstones on the other hand do not show a modulus-porosity trend. These datapoints fill the space between the contact and non-contact cement theoretical trajectories (the latter calculated for quartz rock at 29 MPa effective pressure). Similarly, in the permeability-porosity plane these rocks fill the space between the Troll and Oseberg datapoints, and a permeability-porosity trend is absent.

As we mentioned before, both HRZ and LRZ rocks are quartz-cemented and have very close mineralogy. Based on these facts, we assume that both the modulus-porosity and permeability-porosity non-uniqueness (Figure 4) is due to the varying amounts of contact and non-contact cement.

DIAGNOSING ROCK FOR NON-CONTACT CEMENT

In order to calculate the amount of the non-contact cement from sonic and porosity we use a model where a high-porosity sandstone has an idealized texture. Its basic framework is a random dense pack of identical spherical grains at some critical porosity ϕ_c which may vary between 0.36 and 0.4 (Nur et al., 1998). Every grain is identically and evenly enveloped by a layer of contact cement, and the rest of the solid phase (additional to the grains and contact cement) forms non-contact cement deposited in the pore space away from grain contacts (Figure 5a).

One is unlikely to encounter such an idealized picture in a thin section. However, this is a way to build effective medium models, some of which have been effectively used to model granular rocks (e.g., Dvorkin and Nur, 1996; Moos et al., 1997).

Let us now consider a datapoint in the modulus-porosity plane that lies below a theoretical contact cement trajectory (Figure 5b). We assume that the non-contact cement does not contribute to the stiffness of this rock. Therefore, its elastic modulus is identical to that of a higher porosity (ϕ_{cem}) rock of the same texture but without the

non-contact cement. The corresponding datapoint is the horizontal projection (in the modulus-porosity plane) of the original one onto a contact-cement trajectory (Figure 5b).

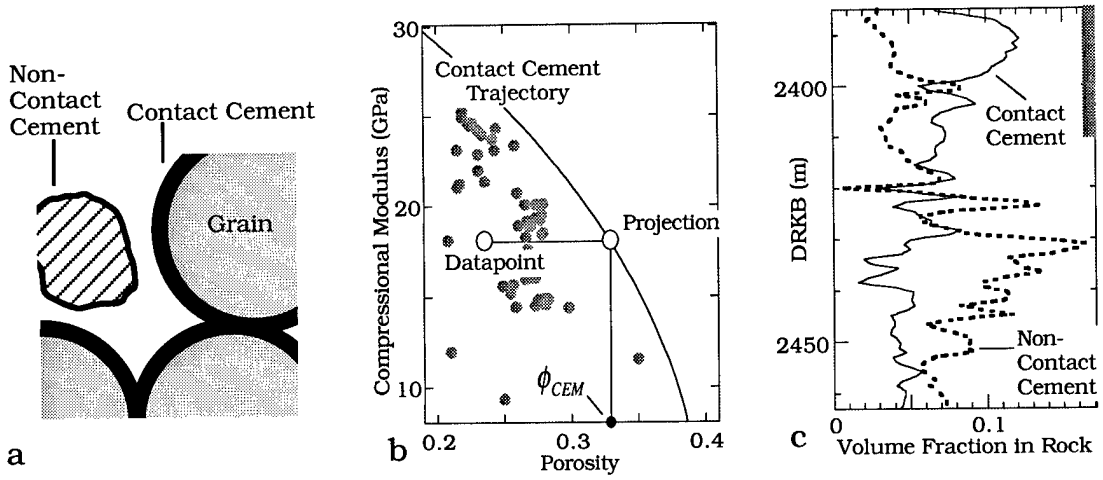

Figure 5. a. Idealized picture of granular rock with contact and non-contact cement. b. Calculating the amount of non-contact cement. Gray symbols show some scattered datapoints. c. Volumetric fraction of contact (solid line) and non-contact (dotted line) cement versus depth in well 15/9-16. Gray vertical bar shows the extent of HRZ.

Volume balance gives the following relations between the porosity of the datapoint (ϕ), its projection on the contact-cement trajectory (ϕ_{cem}), critical porosity (ϕ_c), and the volume fractions of the contact (f_{cc}) and non-contact (f_{ncc}) cement in rock:

$$f_{cc} = \phi_c - \phi_{cem}; f_{ncc} = \phi_c - \phi - f_{cc}. \quad (1)$$

The contact-cement trajectory can be plotted using equations in Dvorkin and Nur (1996); it depends on the elastic moduli of grains and cement, and on the chosen critical porosity value. An additional input parameter is the average number of contacts per grain in the original sphere pack (n). It may vary between 9 and 8.

In the case under examination we choose ϕ_c = 0.38 (average between 0.36 and 0.4) and n = 8.5. Because the grains and contact cement are predominantly quartz, we plot the contact-cement trajectory for quartz-cemented quartz grains (Figure 5b). In

calculating this trajectory, we use 38 GPa and 44 GPa for the bulk and shear moduli of quartz, respectively (Carmichael, 1990).

This trajectory can be statistically fitted (with correlation coefficient about 1) by the equation

$$1.037\sqrt{0.38-\phi_{cem}} = -0.0013 + 0.0134M + 4.3\cdot 10^{-5}M^2, \qquad (2)$$

where M is the compressional modulus of the dry contact-cemented rock. The contact-cement trajectory for any set of input parameters can be obtained from Dvorkin and Nur (1996). Then it can be statistically fitted by an equation similar to Equation (2).

Now we can combine Equations (1) and (2) to arrive at a formula that relates the volumetric fractions of the contact and non-contact cement to the dry-frame compressional modulus and porosity:

$$f_{cc} = 0.93(-0.0013 + 0.0134M + 4.3\cdot 10^{-5}M^2)^2,\ f_{ncc} = 0.38 - \phi - f_{cc}. \qquad (3)$$

These fractions, as calculated for well 5/9-16 (using the dry-frame compressional modulus from fluid substitution) are given in Figure 5c. The contact cement dominates in HRZ whereas the non-contact cement is prevalent in LRZ.

This diagnostic can be immediately used to assess the strength of the rock: clearly the larger the amount of contact cement the stronger the rock (at the same porosity). This effect could be clearly seen in the Troll and Oseberg example (Figure 1). The Troll samples that do not have contact cement are friable sands (Blangy, 1992), whereas the Oseberg samples show significant structural integrity (Strandenes, 1991). In the case under examination, our diagnostic is also consistent with the rock's strength: Nadeau (1998) states that quartz cementation progressed more readily in HRZ and is associated with intervals less prone to sand production.

PERMEABILITY TREND

In Figure 6a we plot the logarithm of permeability (k) versus the volumetric fraction of the non-contact cement. A linear trend is evident (as opposed to the absence of such in Figure 3). The linear-fit equation for this trend is

$$\mathrm{Log}_{10}k = 3.3 - 19.46 f_{ncc};\ R = 0.85. \tag{4}$$

The correlation slightly improves if the permeability is normalized by the grain size (d) squared (Figure 6b):

$$\mathrm{Log}_{10}(k / d^2) = 4.8 - 20.47 f_{ncc};\ R = 0.86. \tag{5}$$

Such normalization is often used to improve permeability trends because permeability strongly depends on the grain size (e.g., Bourbie et al., 1987). In our case this improvement is small due to a relatively uniform grain size distribution in the interval (between 0.15 and 0.25 mm).

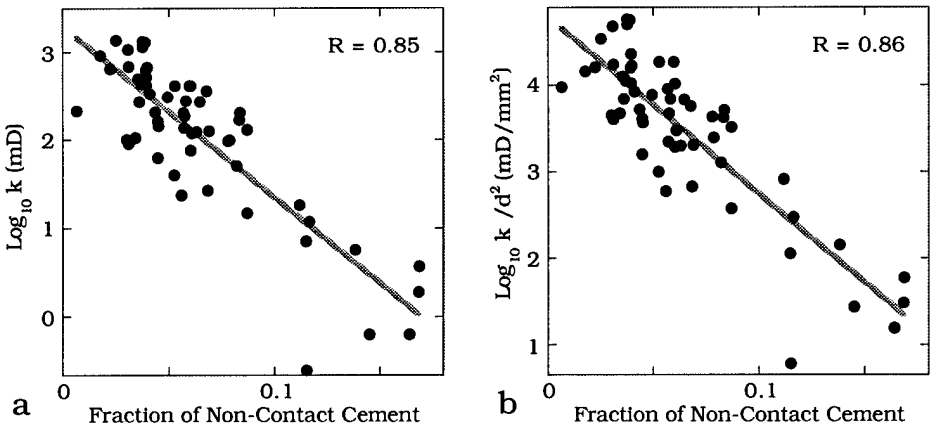

Figure 6. Permeability (a) and permeability normalized by grain size squared (b) versus the volumetric fraction of non-contact cement. Gray lines show best linear fits. Correlation coefficients are given in the graphs.

CONCLUSION AND RECOMMENDATIONS

The high-correlation trends expressed by Equations (4) and (5) can be used to predict permeability from sonic and porosity data. We obtained these trends by using the

amount of non-contact cement to quantify the variability of rock texture. This confirms our initial hypothesis that textural variability in rock, specifically, the amount of the non-contact cement, can be responsible for non-uniqueness in permeability-porosity trends such as shown in Figure 3. To calculate the amount of the non-contact cement is a way of obtaining a meaningful correlation for permeability.

The method of calculating the amount of contact and non-contact cement presented here is in fact a method of diagnosing the texture of high-porosity sandstone from well-log data. Such diagnostic is important not only for obtaining a usable correlation for permeability but also for assessing the strength of rock and its susceptibility to sanding.

Equation (2) is not universal. In every separate case study it has to be re-derived from the appropriate contact-cement trajectory where the elastic moduli of the grains and cement are selected according to mineralogy or within reasonable ranges. The "free" parameters ϕ_c and n can be varied within reasonable (narrow) ranges until the best correlation, such as Equation (4), is obtained.

REFERENCES

Batzle, M., and Wang, Z., 1992, Seismic properties of pore fluids: Geophysics, 57, 1396-1408.

Blangy, J.P., 1992, Integrated seismic lithologic interpretation: The petrophysical basis: Ph.D. thesis, Stanford University.

Bourbie, T., Coussy, O., and Zinszner, B., 1987, Acoustics of porous media, Gulf Publishing Company.

Carmichael, R.S., 1990, Practical handbook of physical properties of rocks and minerals: CRC Press.

Dvorkin, J., and Nur, A., 1996, Elasticity of high-porosity sandstones: Theory for two North Sea datasets: Geophysics, 61, 1363-1370.

Han, D.-H., 1986, Effects of porosity and clay content on acoustic properties of sandstones and unconsolidated sediments: Ph.D. thesis, Stanford University.

Mavko, G., Chan, C., and Mukerji, T., 1995, Fluid substitution: Estimating changes in V_p without knowing V_s: Geophysics, 60, 1750-1755.

Moos, D., Dvorkin, J., and Hooks, A.J., 1997, Application of theoretically derived rock physics relationships for clastic rocks to log data from Wilmington field, CA: Geophysical Research Letters, 24, 329-332.

Nadeau, P.H., 1998, The Sleipner effect: A possible relationship between hydrocarbon charge and the distribution of sandstone reservoir cements: in Mineral diagenesis and reservoir quality -- the way forward, Conference abstracts, University of Cambridge, UK, March 1998, 162.

Nur, A., Mavko, G., Dvorkin, J., and Galmudi, D., 1998, Critical porosity: A key to relating physical properties to porosity in rocks: The Leading Edge, 17, 357-362.

Schlumberger, 1989, Log interpretation principles/applications: Schlumberger Wireline & Testing, Houston.

Strandenes, S., 1991, Personal communication.

Strandenes, S., 1995, Personal communication.

2.3. DIAGNOSING SANDS USING SONIC AND SEISMIC

In collaboration with Per Avseth, Gary Mavko, and Johannes Rykkje

ABSTRACT

At high porosity, velocity in reservoir rocks strongly depends on the position of the intergranular material. Velocity is high if the original grains are cemented at their contacts. It is low if the pore-filling material is placed away from the contacts. In the latter case we have truly unconsolidated sediments. In the former case we have high-porosity cemented rocks. Separating these two rock types is important for hydrocarbon identification. Due to the difference in the rock frame stiffness between the unconsolidated and high-porosity cemented rocks, seismic signatures of the former filled with water can be very close to those of the latter filled with hydrocarbons. This may complicate direct hydrocarbon detection. We separate the two rock types by diagnosing sand using rock physics theory. We conduct such diagnostic on well log data from two wells that penetrate the Heimdal formation (North Sea). We show that the Heimdal formation reservoir is composed of both unconsolidated and cemented high-porosity sands. The initial quartz cementation present in the latter is clearly seen in the cathode-luminescent SEM images. These images, combined with point XRD analysis, confirm our diagnostic that the high-velocity high-porosity sands in Heimdal contain quartz grains surrounded by quartz-cement rims. We find that the two different types of sand which are capped by similar low-impedance shales produce drastically different AVO signatures. The oil-filled high-porosity cemented sand shows a relatively strong zero-offset reflectivity which becomes less positive with increasing offset, while the oil-filled uncemented sand shows a negative zero-offset reflectivity with increasingly negative far-offset response. These results show that (1) rock diagnostic can be conducted not only on the log scale but also on the seismic scale; and (2) taking into account the nature of the rock improves our ability to identify pore fluid from seismic.

INTRODUCTION

Quartz cementation of sands greatly affects porosity, permeability, and seismic properties. Sandstones in continuously subsiding sedimentary basins, such as in the North Sea and the Gulf Coast, tend to have poorly developed quartz cement down to a depth of 2.5 - 3.0 km (Bjørlykke and Egeberg, 1993). Hence, Tertiary sands in the North Sea are usually reported to be poorly consolidated with no (or insignificant quantities of) quartz cement. "Insignificant" is related to volume -- small amounts of quartz cement do not significantly affect porosity. However, only small amounts of cement at grain contacts are needed to considerably stiffen the frame of a rock (Dvorkin and Nur, 1996) and strongly increase velocity. We apply the contact cement concept to study two clean sandstone intervals, both representing the Palaeocene age Heimdal Formation in the North Sea. Both intervals are oil-filled reservoir sands of commercial interest. We diagnose the rock using well log measurements and rock physics theory. We assume that if in the velocity-porosity plane a datapoint falls close to a theoretical line, the internal structure of the rock is similar to the idealized structure used in the model. We find from such diagnostic that one interval is composed of unconsolidated sand, while the other interval is composed of cemented high-porosity sand. Thin-section and SEM images confirm this diagnostic. By studying the seismic signatures of these two different types of clean sands we upscale the log-based diagnostic to the seismic scale.

ROCK DIAGNOSTIC AND CONFIRMATION

We examine two wells -- Well #1 and Well #2. Sonic velocity and gamma-ray are plotted versus depth for both wells in Figures 1a to 1d. Vp is plotted versus porosity in Figures 1d and 1f. Notice that in Well #2 a thick sand interval (gray bar in Figure 1c) is marked by extremely low and constant gamma-ray readings. This sand layer is surrounded by high-gamma-ray shale packages. In Figure 1f, these two lithologies fall

into two distinctive velocity-porosity patterns. In Well #1, unlike in Well #2, we observe a gradual variation of clay content between very clean sand and shale. Only a relatively thin (10 m) sand interval (gray bar in Figure 1a) is identified as a practically clay-free reservoir sand. Because of the gradual variation of clay content in this well, we do not observe (Figure 1e) velocity-porosity patterns as distinctive as in Well #1. These two clean sand intervals (in both wells) represent the same stratigraphic level, although located in different oil fields. They are shown by bold black symbols in Figures 1e and 1f.

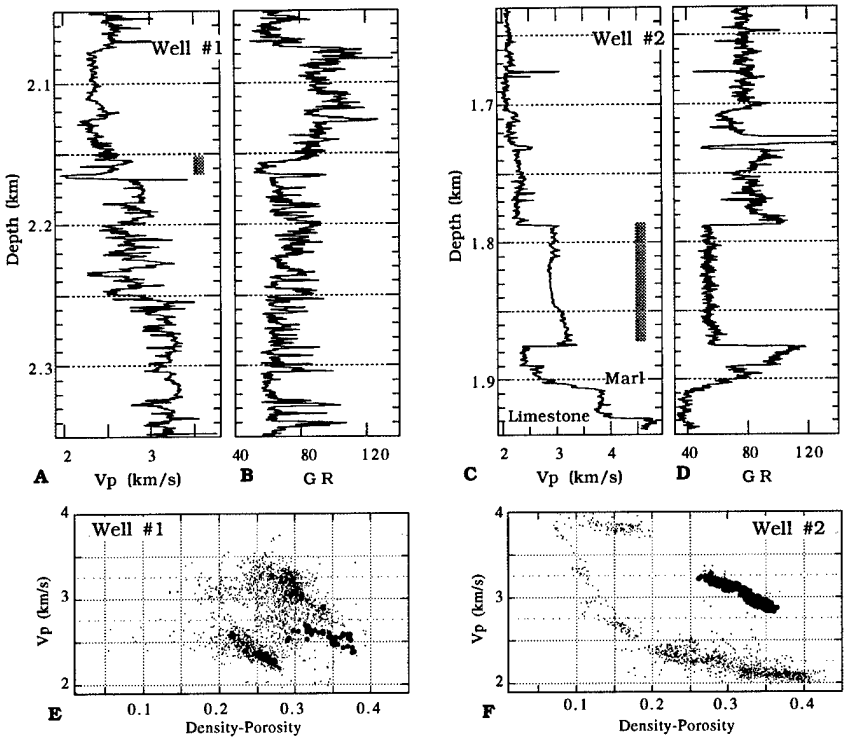

Figure 1. P-wave velocity and gamma-ray versus depth (a-d); and P-wave velocity versus porosity (e and f) for both wells.

To directly confirm this diagnostic, consider the thin sections of two samples from both intervals (Figure 3). The samples have approximately same porosity. They are predominantly quartz. No contact cementation is apparent in both images. The left image (Well #1) shows some organic coating around quartz grains. Consider now two SEM images of a sample from Well #2 (Figure 4). The left-hand image is in back-scatter

light and the right-hand one is in cathode-luminescent light. Notice the V-shaped grain in the middle. No contact cement rim is apparent around this grain in back-scatter light. Cathode-luminescent light reveals a contact-cement rim around this grain. The point XRD analysis shows that both the grain and cement rim are pure quartz. This confirms our diagnostic that the Well #2 sand interval is contact-cemented. The hexagonal crystal shapes in the upper left corner also indicate diagenetic cementation. No cement rims or hexagonal crystal shapes have been found around grains in the sand interval from Well #1. Another direct proof of our diagnostic was that cores extracted from Well #1 appeared as piles of loose sand, whereas those from Well #2 supported external stress.

SEISMIC RESPONSE

To understand how the type of sand (unconsolidated versus cemented) affects the seismic response, we analyze CDP gathers at the well locations. Figure 5a shows the real CDP gather at Well #1 where the picked horizon is at the top of the Heimdal formation. Figure 5b gives a synthetic CDP gather for this well produced by using a 30 Hz zero-phase Ricker wavelet and a log-derived reflectivity series. Both the real and synthetic gathers show reflectivity increasingly negative with increasing offset at the picked horizon. This reflectivity is plotted versus offset (angle), together with the theoretical Zoeppritz line, in Figure 5e. Contrary to Well #1, the top of the Heimdal formation in Well #2 (which is capped by similar shales) produces a strong positive reflector with reflectivity decreasing with increasing offset (Figures 5c and 5d). For this well, the reflectivity is plotted versus offset (angle), together with the theoretical Zoeppritz line, in Figure 5f. The synthetic response is very close to the real data in both wells which means that we can rely on well-log-based rock diagnostic to predict seismic response.

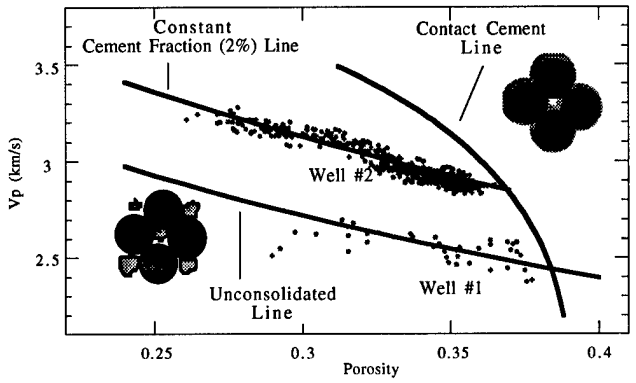

Figure 2. P-wave velocity versus porosity for sand intervals in both wells. Theoretical lines serve to diagnose the rocks.

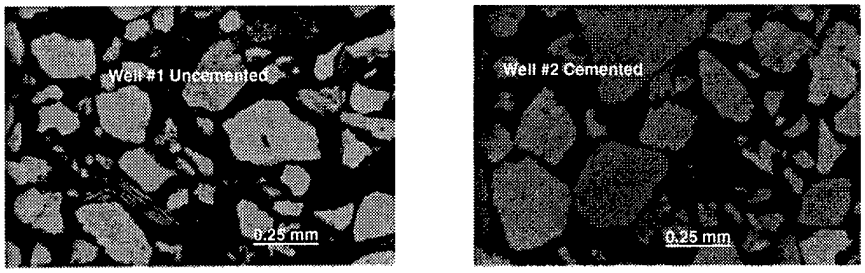

Figure 3. Thin sections of two selected samples from Well #1 (left) and #2 (right).

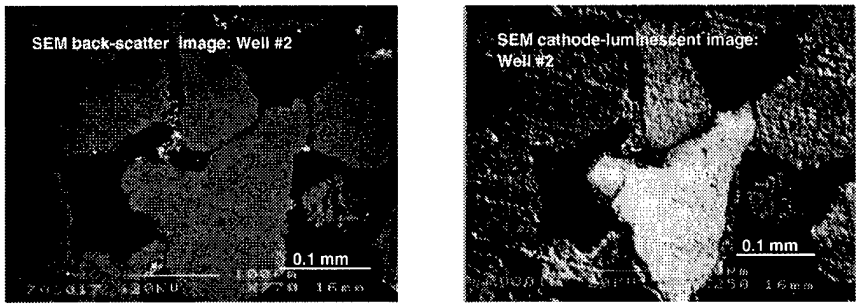

Figure 4. SEM images of a Well #2 sample in back scatter light (left) and cathode-luminescent light (right).

This offset-dependent reflectivity analysis shows that clean sands of the same formation, similar porosity, and with comparable oil saturation produce drastically different seismic response depending on whether they are truly unconsolidated or have initial quartz cementation. Therefore, we can use both normal-incidence and offset-dependent reflectivity to diagnose rock and characterize a reservoir from seismic. Such rock diagnostic may be of great importance because if high-porosity contact-cemented

sands are not separated from truly unconsolidated sands, one may misinterpret a change in seismic signatures caused by this petrographic effect as a pore-fluid effect.

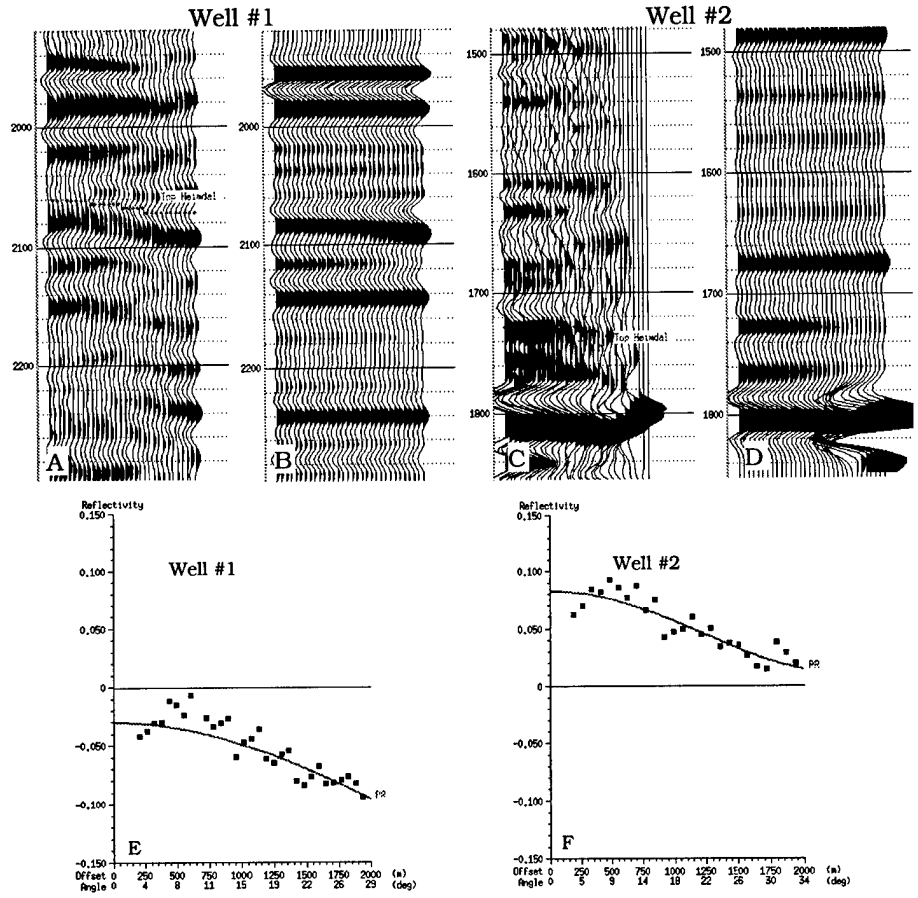

Figure 5. Top. Real (a and c) and synthetic (b and d) CDP gathers. In synthetic gathers, the AVO effect was modeled only at the target zones. Bottom. Real reflectivity versus offset and angle (symbols) and theoretical Zoeppritz lines.

CONCLUSION

Rock diagnostic is important for correctly characterizing prospective reservoirs. Such diagnostic is based on rock physics theory and can be accomplished using well log data. The diagnostic features observed in well log data can be translated into distinctive seismic signatures. Therefore, seismic data can also be used for rock diagnostic given that the stratigraphic unit is resolvable at the seismic scale. In this paper we applied the

diagnostic concept to the Heimdal formation, and were able to discriminate high-porosity cemented from unconsolidated sands both from well logs and seismic.

REFERENCES

Bjørlykke, K., and Egeberg, P.K., 1993, Quartz cementation in sedimentary basins: AAPG Bulletin, v. 77, 1538-1548.

Dvorkin, J., and Nur, A., 1996, Elasticity of high-porosity sandstones: Theory for two north sea datasets, Geophysics, 61, 1363-1370.